JACS
JOURNAL OF THE AMERICAN CHEMICAL SOCIETY
pubs.acs.org/JACS
Article

Bottlebrush Block Copolymers at the Interface of Immiscible Liquids: Adsorption and Lateral Packing

Hong-Gyu Seong, Zichen Jin, Zhan Chen, Mingqiu Hu, Todd Emrick,* and Thomas P. Russell*

Cite This: J. Am. Chem. Soc. 2024, 146, 13000−13009
Read Online

ABSTRACT: Amphiphilic bottlebrush block copolymers (BBCPs), having a hydrophilic bottlebrush polymer (BP) linked covalently to a hydrophobic BP, were found to segregate to liquid−liquid interfaces to minimize the free energy of the system. The key parameter influencing the outcome of the experiments is the ratio between the degree of polymerization of the backbone (N_{BB}) and that of the side-chain brushes (N_{SC}). Specifically, a spherical, star-like configuration results when $N_{BB} < N_{SC}$, while a cylindrical, bottlebrush-like shape is preferred when $N_{BB} > N_{SC}$. Dynamic interfacial tension (γ) and fluorescence recovery after photobleaching (FRAP) measurements show that the BBCP configuration influences the areal density and *in-plane* diffusion at the fluid interface. The characteristic relaxation times associated with BBCP adsorption (τ_A) and reorganization (τ_R) were determined by fitting time-dependent interfacial tension measurements to a sum of two exponential relaxation functions. Both τ_A and τ_R initially increased with N_{BB} up to 92 repeat units, due to the larger hydrodynamic radius in solution and slower *in-plane* diffusivity, attributed to a shorter cross-sectional diameter of the side-chains near the block junction. This trend reversed at N_{BB} = 190, with shorter τ_A and τ_R attributed to increased segregation strength and exposure of the bare water/toluene interface due to tilting and/or wiggling of the backbone chains, respectively. The adsorption energy barrier decreased with higher N_{BB}, due to a reduced BBCP packing density at the fluid interface. This study provides fundamental insights into macromolecular assembly at fluid interfaces, as it pertains to unique bottlebrush block architectures.

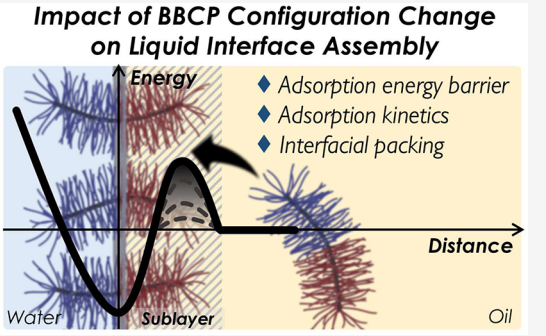

INTRODUCTION

Macromolecular surfactants, referring to polymers containing both hydrophilic and hydrophobic functionality that generate interfacial activity, will segregate to water/oil interfaces to reduce the free energy of the system. Relative to their small-molecule counterparts, macromolecular surfactants offer unparalleled tunability with respect to size, architecture, and composition, enabling a diverse range of chemical and physical properties that contribute to a versatile platform of micro-reactors,[1,2] templates,[3−8] and structures for delivery,[9−12] oil recovery,[13−15] and encapsulation.[16−18] Therefore, a comprehensive understanding of the liquid−liquid interfacial assembly of polymer surfactants is important for advanced materials designs.[19] Recent studies have described the assembly dynamics, packing behavior, and mechanical properties as a function of polymer architecture, including linear,[20−26] star,[27] and bottlebrush (co)polymers.[28−33]

The extensive steric repulsion between densely grafted side-chains of bottlebrush polymers results in backbone stiffening and side-chain extension, and produces physical properties that are distinctly different from their linear analogs.[34−38] Fundamental parameters for tuning bottlebrush architectures include the backbone degree of polymerization (N_{BB}), side chain degree of polymerization (N_{SC}), and grafting density (defined by number of repeating units with polymeric side chain/total repeating units of the backbone). Recent discoveries of bottlebrush polymer assembly in the bulk,[39−42] as thin-films,[42,43] and at liquid−liquid interfaces[28−33] demonstrate that the bottlebrush configuration is crucial to both solid−solid and liquid−liquid interfacial assembly. Factors such as random vs block structure, N_{BB}, N_{SC}, and grafting density influence interfacial assembly kinetics and surfactant properties. For example, Verduzco[44] and Sing[45] combined scattering techniques with viscosity measurements to study the solution configuration of bottlebrush homopolymers as a function of N_{BB} and N_{SC}. Their findings showed the importance of the N_{BB}:N_{SC} ratio, finding star-like (spherical) shapes when $N_{BB} < N_{SC}$, worm-like configurations (flexible cylinders) when $N_{BB} \gg N_{SC}$, and a star-to-bottlebrush transition when $N_{BB} \sim N_{SC}$. This variation in the solution configuration is important for controlling assembly dynamics and packing at liquid−liquid interfaces.

Received: December 7, 2023
Revised: April 29, 2024
Accepted: April 30, 2024
Published: May 6, 2024

https://doi.org/10.1021/jacs.3c13817
J. Am. Chem. Soc. 2024, 146, 13000−13009

In prior work, the stability of water-in-oil emulsions prepared using *bottlebrush random copolymers* (BRCPs) as a function of N_{BB} and N_{SC} was described by Matyjaszewski and co-workers,[30] where the mole fraction and length of poly(ethylene oxide) (PEO) side-chains proved important for stabilizing water/xylene emulsions. Notably, emulsions stabilized by BRCPs were more stable than those with their linear analogue (PEO-*b*-poly(*n*-butyl methacrylate)); among branched polymers (both star- and bottlebrush-like), BRCPs with lower N_{BB} produced smaller droplets. We recently reported the influence of N_{BB} on the initial interfacial assembly kinetics, packing behavior, and *in-plane* diffusion dynamics of BRCPs,[28] finding that larger N_{BB} results in slower initial assembly, involving reconfiguration of randomly distributed (hydrophilic−hydrophobic) side-chains, and faster *in-plane* diffusion dynamics.

Bottlebrush block copolymers (BBCPs) present a distinctly different set of considerations. In contrast to BRCPs, BBCPs do not require extensive side-chain reconfiguration for interfacial assembly due to the intrinsic separation of hydrophilic and hydrophobic domains. A distinctive feature of the BBCP case, in comparison to the bottlebrush homopolymer, is that the solvent quality (good, theta, or poor) for each block imparts a unique local chain conformation. Under selective solvent conditions, this drives BBCP assembly into well-defined nanostructures.[46−49] For example, using amphiphilic BBCPs to template porous microspheres, Song and co-workers demonstrated that the interfacial instability of water/oil interfaces to result in spontaneous emulsification.[8] Emulsion droplet diameters and therefore microsphere pore sizes were adjusted with N_{BB}: As N_{BB} increased, the lower curvature of the water/toluene interface produced larger pores. The backbone rigidity, which is related to the BBCP grafting density, proved to be crucial for tuning pore sizes with N_{BB}; incorporating a flexible segment between two side-chain blocks led to a broader pore size distribution. This and other studies[47,48,50−57] demonstrate that the bottlebrush polymer architecture represents an emerging opportunity to impart the macroscopic properties of emulsions and the morphologies of the resultant nanoscale structures.

As illustrated in Figure 1A, the axial length (l) and diameter (d) of both BBCPs and BRCPs increase with N_{BB} and N_{SC}, respectively. For BRCPs, interfacial reconfiguration establishes hydrophilic-rich and hydrophobic-rich domains for adsorption to a fluid interface, in which the backbone orientation must be parallel to the water/oil interface. As N_{BB} increases, the projection area per polymer increases, reducing the packing efficiency.[28] In contrast, for BBCPs, the backbone orientation at the fluid interface is prone to be perpendicular to the water/oil interface, making their projection area per molecule more sensitive to N_{SC} than N_{BB} (Figure 1B). We note, however, that the bottlebrush polymer configuration at the liquid interface may differ from the schematic depiction in Figure 1B, which is due to the fact that both backbone and side-chains are not in the superstretched limit but rather that they have flexibility to some extent.[49,58] Thus, although prior studies examined the relationships between BBCP architecture and solution assembly, key fundamental questions remain concerning BBCPs at fluid interfaces, including the impact of N_{BB} on: 1) *in-plane* diffusivity; 2) bending rigidity of the BBCP assembly; and 3) adsorption energy barriers.

Here, we describe the assembly of BBCPs at fluid interfaces as a function of N_{BB}. By maintaining the N_{SC} of the two

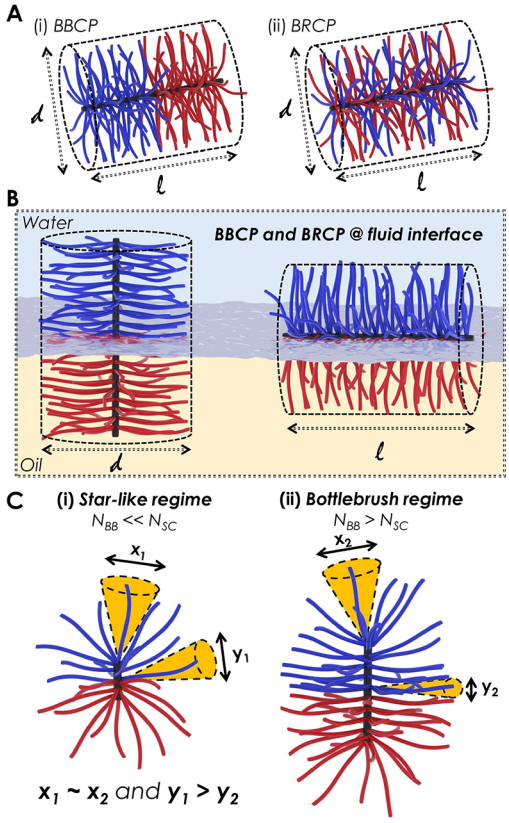

Figure 1. Schematic illustrations of (A) BBCPs and BRCPs with hydrophilic (blue) and hydrophobic (red) side-chains; (B) bottlebrush orientation at the water/oil interface; (C) schematic representation of the volume occupied by a side-chain located at the BBCP backbone chain-end (diameters x_1 and x_2) or block junction (diameters y_1 and y_2).

different side-chains and fixing the molar ratio of hydrophilic−hydrophobic side-chains at 1:1, we used the N_{BB}:N_{SC} ratio to tailor the macromolecular shape from spherical to flexible cylindrical. The time-dependent interfacial tension (IFT, γ) was measured by tensiometry, giving information on assembly dynamics, packing efficiency, and adsorption energy. Fluorescence recovery after photobleaching (FRAP) experiments provided information about the *in-plane* diffusion of BBCPs at the fluid interface. These studies establish fundamental structure−property relationships between BBCP architectures and their dynamics at fluid interfaces.

RESULTS AND DISCUSSION

Synthesis and Solution Chain Configuration of BBCPs. Macromonomers containing poly(dimethylsiloxane) (PDMS) and poly(ethylene oxide) (PEO) side-chains were synthesized by amidation or esterification of *N*-(carboxyhexyl)-*cis*-5-norbornene-*exo*-2,3-dicarboxyimide with PDMS-NH_2 or PEO−OH, yielding NB-PDMS and NB-mPEO, respectively[28] (synthetic and characterization details provided in the Supporting Information, Figures S1 and S2). Using these macromonomers, the amphiphilic BBCPs containing PDMS and PEO side-chains were synthesized by ruthenium benzylidene-initiated ring-opening metathesis polymerization (ROMP) with $(H_2IMes)(Cl)_2(pyr)_2RuCHPh$).[59] This approach resulted in high monomer conversion and fast polymerization kinetics while ensuring 100% grafting density, yielding BBCPs with one side-chain per repeat unit. For BBCP

https://doi.org/10.1021/jacs.3c13817
J. Am. Chem. Soc. 2024, 146, 13000−13009

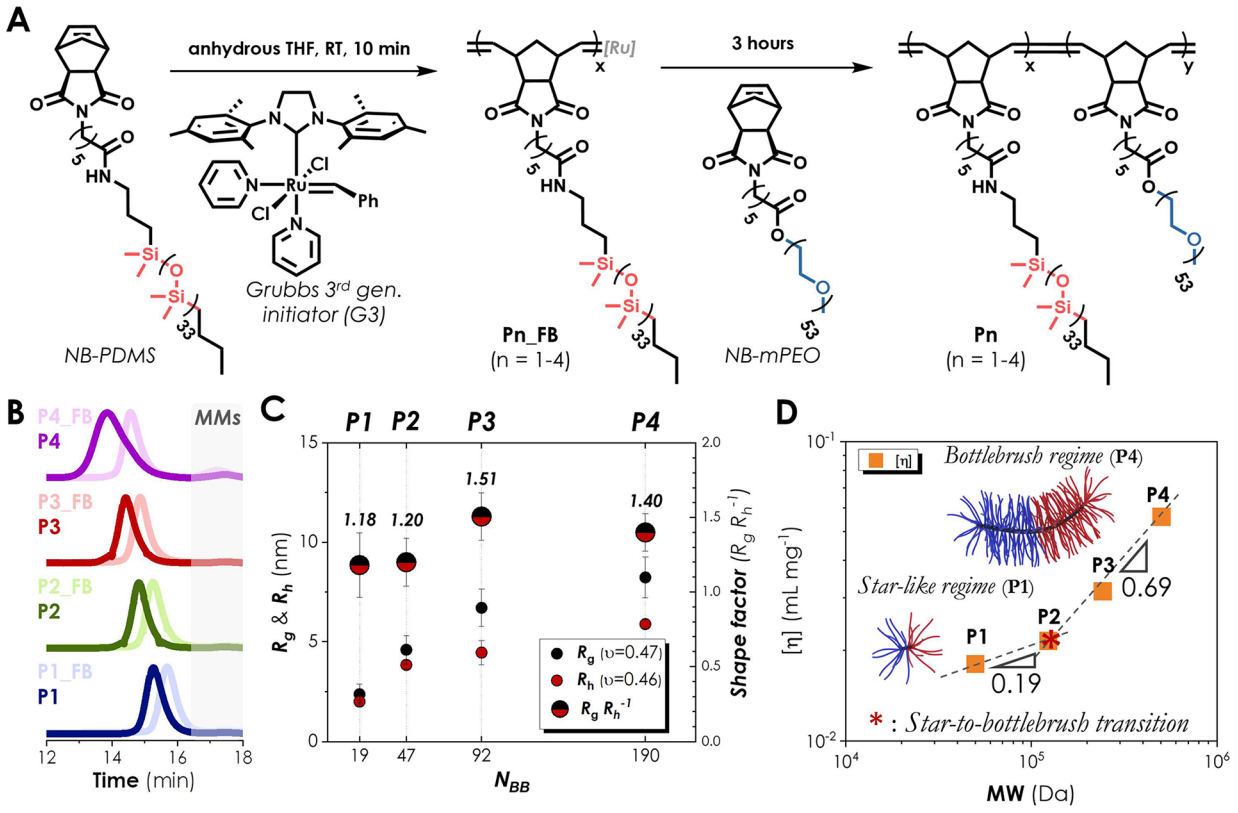

Figure 2. (A) Synthesis of BBCPs by ROMP of NB-PDMS and NB-mPEO. (B) MALLS-SEC traces of different N_{BB} of BBCPs. (C) Summary of R_g, R_h, and shape factor (defined by R_g R_h^{-1}) as a function of N_{BB} of BBCPs; υ denotes the scaling exponent of R_g or R_h vs $N_{BB}{}^{\upsilon}$. (D) Intrinsic viscosity vs MW in the log−log plot, which showed star-to-bottlebrush transition around **P2**.

Table 1. Characterization data for BBCPs P1−P4

entry	target N_{BB} ([MM]/[G3])	$M_{n,theo}$ (kDa)	f_{PEO} (%)	actual N_{BB}[a]	$M_{n,MALLS\text{-}SEC}$ (kDa)	$M_{w,MALLS\text{-}SEC}$ (kDa)	PDI
P1	20	53.0	49.6	19	50.0	59.2	1.18
P2	50	132.0	50.1	47	123.7	144.0	1.16
P3	100	265.0	49.8	92	242.6	289.3	1.19
P4	200	530.0	49.5	190	502.9	778.8	1.54

[a]Actual N_{BB} denotes that each bottlebrush block copolymer has polymeric side-chains with a number of "actual N_{BB}" in average.

preparation, we began by performing ROMP of NB-PDMS in anhydrous THF, which revealed first-order polymerization kinetics and nearly quantitative conversion in just 5 min (Figure S3). Then, the addition of NB-mPEO to the active chain-end produced the desired BBCP, with evidence from size-exclusion chromatography (SEC), where growth of the second block produced peaks at shorter elution times corresponding to higher molecular weight polymer (Figure 2B). As anticipated for a controlled polymerization of this type, adjusting the macromonomer:initiator ratio (or [MM]:[G3]) exerted control over N_{BB} of the resultant BBCPs. Table 1 summarizes BBCP characterization, including molecular weight and polydispersity index (PDI) values estimated by size-exclusion chromatography (SEC). The molecular weight and PDI of the resulting BBCPs range from 47 to 503 kDa and 1.16 to 1.54, respectively (Tables 1 and S1). The higher PDI value for **P4** is likely due to catalyst deactivation, which may impact polymer diffusivity and interfacial assembly behavior.[60]

To investigate the BBCP solution configuration, dynamic light scattering (DLS) and static light scattering (SLS) experiments were performed. DLS analysis of BBCPs with different N_{BB} values (Figures S8 and S9) showed a shift in the size distribution peak of R_h toward larger values, indicating an overall increase in size, while SLS measurements of the radius of gyration (R_g, Figure S10) allowed calculation of the shape factor (R_g R_h^{-1}, a dimensionless value that reflects the shape and mass distribution of scattering objects in solvent).[61] For **P1** (N_{BB} 19) and **P2** (N_{BB} 47), shape factors of 1.18 and 1.20 resemble those of a spherical star polymer (1.14 in the theta condition), as predicted by Zimm theory (Figure 2C).[62] In the $N_{BB} < N_{SC}$ regime, increasing N_{BB} did not significantly alter the aspect ratio but did increase the local density of side-chains, confirming the expected spherical shape in toluene, consistent with a star-like regime.[62,63] **P3** (N_{BB} 92) had the highest shape factor of 1.51, similar to that of a randomly branched polymer (1.7, Zimm theory, theta condition, $N_{BB} > N_{SC}$) with a rigid cylindrical configuration.[62] As N_{BB} increased further in **P4** ($N_{BB} \gg N_{SC}$, N_{BB} 190), the shape factor decreased to 1.40, attributed to backbone flexibility or wiggling. We note that Sing and co-workers similarly described a rigid cylindrical shape of bottlebrush homopolymers with N_{SC} = 30 (poly(L-lactic acid)) at N_{BB} = 87, based on intrinsic viscosity, R_g, and R_h measurements, and coarse-grained simulations.[45] The observed trend in Figure 2C, illustrating the shape factor,

https://doi.org/10.1021/jacs.3c13817
J. Am. Chem. Soc. 2024, 146, 13000−13009

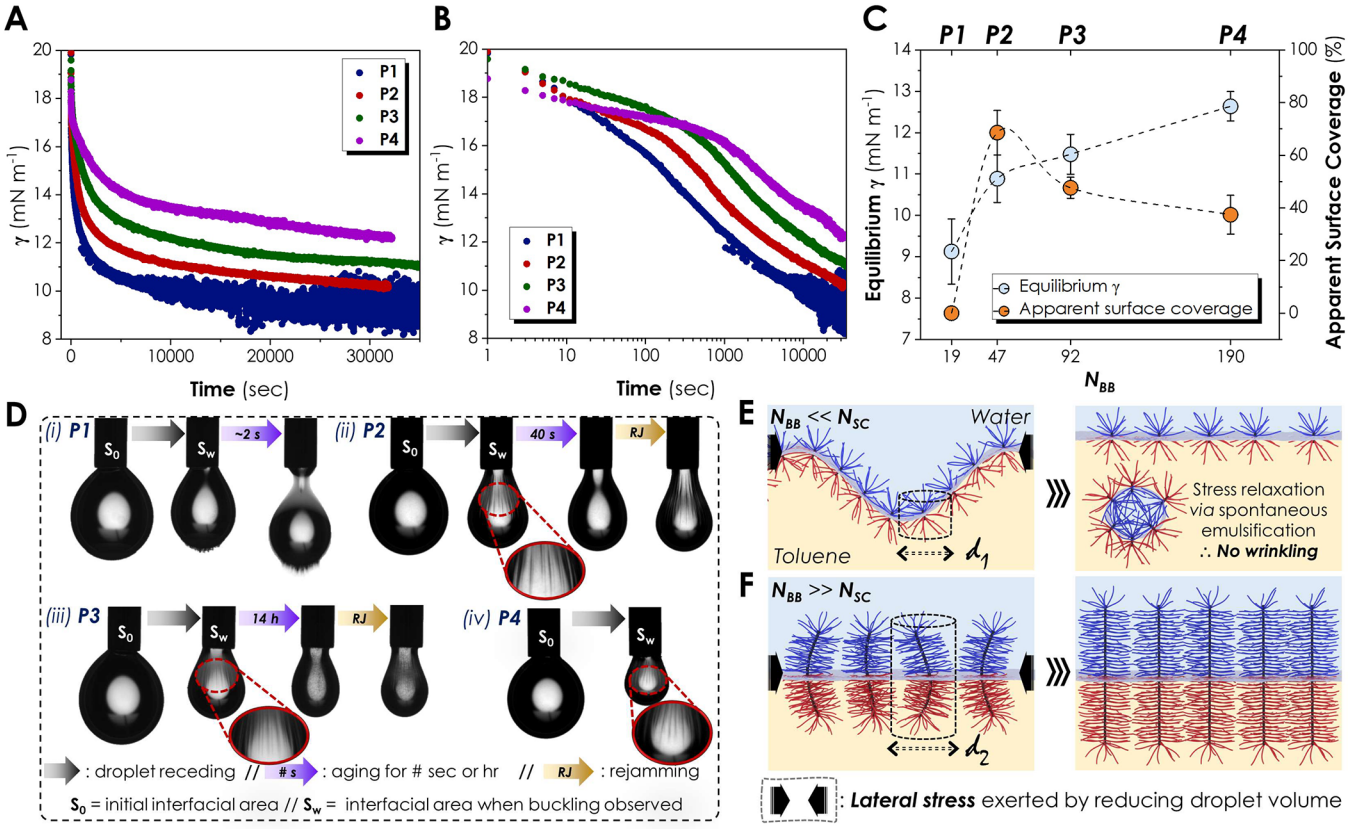

Figure 3. Dynamic interfacial tension measurement with (A) linear−linear and (B) linear-log plot as a function of N_{BB} (**P1**−**P4**). (C) Summary of the equilibrium IFT and ASC as a function of N_{BB} of BBCP. (D) Snapshots of droplets at different stages of **P1**−**P4**, where the first snapshot for each BBCP was taken at the equilibrium stage. Schematic illustrations of (E) lower N_{BB} and (F) higher N_{BB} BBCPs at the water/toluene interface.

aligns with the "asphericity" vs molecular weight plot described by Sing, from 0 (spherical) to 1 (elongated). In their study, increasing N_{BB} initially led to a decrease in asphericity when $N_{BB} < N_{SC}$, followed by an increase when $N_{BB} > N_{SC}$, consistent with the trend observed in the shape factor (Figure 2C). The intrinsic viscosity ($[\eta]$) proved sensitive to shape change, with a sharp transition in the scaling exponent near **P2** in the $[\eta]$ vs molecular weight plot (Figure 2D), indicative of a star-to-bottlebrush transition ($N_{BB} \sim N_{SC}$).[45] From the aforementioned studies and our light scattering experiment results, **P1** assumes a spherical configuration, while **P2** is ellipsoidal, with both falling in the star-like regime. **P3**, in contrast, lies in the bottlebrush regime with a rigid cylindrical shape, while the bottlebrush configuration of **P4** may be viewed as a flexible cylinder. Characterization data of BBCP in solution, including dynamic and static light scattering and intrinsic viscosity, are in Figures S8−S11.

Interfacial Tension (IFT) Measurements and Jamming Experiments. To assess the fluid−fluid interface properties of BBCPs with different N_{BB} values, we conducted pendant drop tensiometry experiments with droplets of DI water (10 μL, pH 5.7) suspended in 1 mg mL^{-1} toluene solutions of BBCPs **P1**−**P4**. The droplet shape was monitored over time and the resulting principal curvatures were fit to the Young−Laplace equation to determine dynamic interfacial tension (γ) values.[64] As N_{BB} increased from **P1** to **P4**, the quasi-equilibrium γ (as $-d\gamma/dt$ approaches 0) also increased, indicating less efficient polymer coverage at the droplet interface (Figure 3A). The rate of change of γ at t = 1 s ($-d\gamma/dt_{t=1s}$) showed a weak correlation with N_{BB} (Figure S12E), presumably due to a superconvection of BBCPs when the water droplet was injected into the BBCP-containing toluene solution. However, $-d\gamma/dt$ at t = 50−100 s decreases with increasing N_{BB} (Figure S12F), which is attributed to slower diffusion for larger N_{BB} values and is consistent with the trend observed in Figure S8 (i.e., where the change in R_h as a function N_{BB} is shown, Figure S9).

The observed increase in γ with N_{BB}, as shown in Figure 3C, can be understood by considering the solution conformation of BBCPs. **P1** had the lowest γ, decreasing to ∼9 mN m^{-1} at long times. As the configuration of the BBCP transitions from spherical (**P1**) to ellipsoidal (**P2**) to rigid cylindrical (**P3**), the BBCP can adopt a *tilted* configuration at the fluid interface due to thermal fluctuations, increasing the projected area per macromolecule at the interface and, therefore, an increase of γ. For **P4**, the added flexibility of the cylindrical structure will also allow for *wiggling* of the backbone, exposing even more of the bare water/toluene interface and a higher value of γ (Figure 3F).

This assessment is supported by the apparent surface coverage (ASC, Figure 3C), determined from the ratio of the interfacial area of the droplet (S_W) when wrinkling occurs (during reduction of droplet volume) to the initial interfacial area (S_0), as shown in Figure 3D. When a quasi-equilibrium γ was achieved, the surface area of the W/O interface was reduced by receding the syringe and hence droplet volume. S_W was recorded when wrinkles at the W/O interface were observed during the receding process. Even though **P1** has the lowest γ, no wrinkling was observed (Figure 3C). Notably, spontaneous emulsification occurred during the interfacial

https://doi.org/10.1021/jacs.3c13817
J. Am. Chem. Soc. 2024, 146, 13000−13009

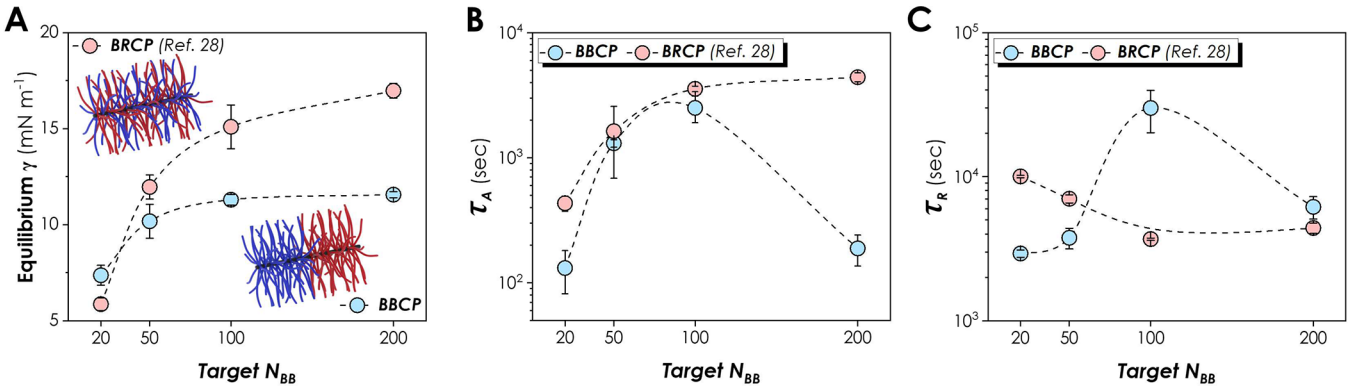

Figure 4. (A) Comparison of the equilibrium γ of BBCP (blue) and BRCP (red, ref 28). Characteristic relaxation time related to the (B) macromolecular adsorption and (C) reorganization of BBCPs and BRCPs. Adapted with permission from ref 28, Copyright 2022 Wiley-VCH Verlag GmbH and Co. KGaA, Weinheim.

tension (IFT) measurement for **P1**, but not for **P2**−**P4**. The lower bending modulus of **P1** assembly results in a higher interfacial curvature compared to larger BBCPs.[6,8] The flexibility of this assembly induces undulations of the fluid interface as the areal density of **P1** increases and the interfacial tension decreases, leading to spontaneous emulsification (Figure 3E).[65,66] Thus, despite the high binding energy imparted by the amphiphilic structure of **P1**, spontaneous emulsification continually reduces the number of polymers at the interface, thereby avoiding wrinkling. Increasing N_{BB} from 19 to 47 removes the tendency for spontaneous emulsification due to the higher bending modulus of the interface. Consequently, upon reduction of the droplet volume, wrinkling results in an ASC of ∼69% (Figure 3C,D). As N_{BB} increases, we expected ASC to likewise increase due to the higher binding energy per BBCP and higher bending modulus of the resultant assembly. On the contrary, a substantial decrease in ASC was observed, from 69% (**P2**) to 37% (**P4**), likely due to a lower packing density of BBCPs with higher N_{BB} due to thermally induced backbone *tilting*. Additionally, macromolecular *wiggling* in **P4** further contributes to the decrease in the ASC (Figure 3F). In our previous work, bottlebrush random copolymers (BRCPs) with similar N_{BB} values exhibited no such wrinkling (for all BRCPs investigated) and instead produced spontaneous emulsification at even lower polymer concentrations (0.1 mg mL^{-1}).[28] Thus, BBCP orientation normal to the fluid interface produces a more robust droplet interface with a significantly higher bending modulus.

For the BBCP interfacial assemblies described here, the wrinkles created by interfacial jamming are not fixed, but rather relax as they reorganize over time. For example, for **P2**, when wrinkling occurred at the droplet interface, relaxation occurred in <1 min, while for **P3**, the relaxation required 14 h, despite its lower ASC (Figure 3D). This extended relaxation time likely arises from the higher local density of side-chains near the block junction (Figure 1C) that contribute hard particle-like properties[67] and thus slower stress relaxation kinetics.

Bottlebrush Polymer Interfacial Assembly: Impact of Block vs Random Architecture. The results described to this point suggest the bottlebrush polymer microstructure to be pivotal for determining assembly characteristics at fluid interfaces, in accord with Figure 1B whereby the block architecture assembles normal to the fluid interface, while the random architecture lies parallel to the interface. Here we compare BBCP assembly to our prior report on random bottlebrush structures containing similar PEO and PDMS side-chains, performing experiments with 0.001 mg mL^{-1} BBCP solutions in toluene. The dynamic interfacial tension at the water/toluene interface was determined using pendant drop tensiometry (10 μL water droplet, pH 5.7, Figure S13A). For BBCPs, the equilibrium γ ranged from 7 mN m^{-1} (**P1**, N_{BB} 20) to 11 mN m^{-1} (**P4**, N_{BB} 200), as shown in Figure 4A. Overall, the BBCPs exhibit relatively similar equilibrium γ values, suggesting a similar projected area per macromolecule at the fluid interfaces, which in turn supports their normal orientation (Figure 1B). In contrast, for BRCPs, γ increased from 6 to 17 mN m^{-1} when going from N_{BB} 20 to 200, since the *in-plane* orientation of the backbone at the interface decreases packing efficiency at higher aspect ratios. γ vs time plots analyzed by fitting to a sum of two exponential relaxation functions, revealed two distinct relaxation times associated with initial *adsorption* and the subsequent *reorganization* kinetics (Figure S13B−E). These insights highlight the adsorption mechanism of bottlebrush polymers of distinct architectures, where the architecture must markedly alter the characteristic relaxation time. Unlike BRCPs, the BBCP block structure does not require significant side-chain reconfiguration upon approaching the fluid interface due to its inherent division into hydrophilic-rich and hydrophobic-rich domains. The first characteristic relaxation time associated with adsorption (τ_A) to fluid interfaces follows similar trends for the BRCPs and BBCPs for N_{BB} = 20 to 100, where the BBCP exhibited much shorter τ_A, demonstrating the importance of BRCP reconfiguration at the initial stage of assembly. However, for target N_{BB} = 200, the segregation of the two chemically distinct blocks for the BBCPs, absent any significant reorganization of the chain at the interface, led in faster adsorption (Figure 4B). The second characteristic relaxation time (τ_R) is associated with the reorganization of copolymers already present at the interface. τ_R for the BRCPs with lower N_{BB} values have longer relaxation times in keeping with their higher packing efficiency reflected in the lower γ (Figure 4C). For the BBCPs, τ_R increased with N_{BB} from 20 to 100, then decreased at N_{BB} = 200 (Figure 4C). The longer τ_R is to be expected, since macromolecular size increases and the shape of the molecule is of secondary importance. However, the decline in τ_R at highest N_{BB} may reflect a transition from rod-like to flexible cylinder. When N_{BB} increases from 20 to 50, a star-like configuration persists, but the diameter of a cross-section of side-chains near the block

https://doi.org/10.1021/jacs.3c13817
J. Am. Chem. Soc. 2024, 146, 13000−13009

junction decreases ($y_1 > y_2$ in Figure 1C), due to side-chain stretching. At the quasi-equilibrium stage, intermolecular steric repulsion, resulting from the increase in N_{BB} ($y_1 > y_2$, Figure 1C), governs *in-plane* reorganization of the assembled BBCPs. Therefore, reorganizing BBCPs of higher N_{BB} values (e.g., N_{BB} 100) is slower relative to the less-sterically congested and softer BBCPs (e.g., N_{BB} 19). However, when N_{BB} increases further to 190, *wiggling* of the entire chain (Figure 2D) would expose the bare water/toluene interface (Figure 3F), providing more interfacial area for reorganization (Figure 4C) and thus shorter τ_R.

In-Plane Diffusion Dynamics of Bottlebrush Block Copolymers. To further evaluate the dynamics of BBCP reorganization at the fluid interface, fluorescence recovery after photobleaching (FRAP) experiments were performed, which probe the diffusion of labeled-BBCPs at the interface.[68] For these experiments, Rhodamine-B-functionalized BBCPs ($\mathbf{P1_{RB}}$–$\mathbf{P4_{RB}}$) were synthesized with the same targeted N_{BB} values as those of **P1**–**P4**. Details of the polymer synthesis, emulsion preparation, FRAP experiments, and diffusion coefficient calculations are given in Figure S6, S7, and S14. The *in-plane* diffusion coefficients derived from these experiments ($D_{in\text{-}plane}$, Figure 5A) were distinctly nonmonotonic going from **P1** to **P4**. $D_{in\text{-}plane}$ decreased from 7×10^{-12} to 2×10^{-12} m^2 s^{-1} with increasing N_{BB} (18 to 88), attributed to the decreased cross-sectional diameter of side-chains near the block junction and the shorter interside-chain distance ($ID_1 > ID_2$, Figure 5B, (i)). Inverting this initial trend, BBCPs with N_{BB} 190 showed a higher γ and lower ASC due to backbone *wiggling* (Figure 3C,F). The unoccupied water–toluene interface generated by this backbone *wiggling* facilitates *in-plane* diffusion. As a result, the diameter of the projection area per macromolecule of $\mathbf{P4_{RB}}$ (d_2) is greater than that of the lower N_{BB} BBCPs (d_1), leading to faster *in-plane* diffusivity (Figure 5B, (ii)). These findings align well with characterization of γ vs time (Figure 3A), providing further support for our understanding of the key impact of bottlebrush configuration on relaxation time.

Adsorption Energy Barrier Calculations. In an effort to quantify our understanding of the fundamental interfacial assembly behavior of BBCPs, we consider the energetic barriers associated with interfacial adsorption. Initially, the water/toluene interface is unoccupied, allowing BBCPs to diffuse to and adsorb at the interface, an overall free energy reduction. Successful BBCP interfacial adsorption depends on the orientation of the diffusing macromolecules since this impacts contact of the PEO block and the fluid interface. As the system approaches equilibrium, and available fluid interfacial area decreases, a significant energy barrier (ΔG_{aeb}, where *aeb* stands for an adsorption energy barrier) for PEO penetration into the BBCP assembly must be overcome (Figure 6A). This barrier must include effects of interbottlebrush repulsion and unfavorable PEO–PDMS interactions, as reflected in the Flory–Huggins interaction parameter between PEO and PDMS (thin-film $\chi_{PEO/PDMS} \sim 0.225$ at room temperature).[69] We define a distance between the junction point of the BBCP and the plane of the interface (sublayer, Figure 6A) that reflects the distance at which BBCPs approaching the interface begin to experience repulsive forces from BBCPs already present at the interface.

To quantify ΔG_{aeb} for BBCP interfacial assembly, we utilized the theroretical framework of Ward and Tordai[70] on the diffusion and assembly behavior of interfacially active molecules from bulk (solution) to a liquid interface, or *vice versa*:

$$\Gamma(t) = 2c_0\sqrt{\frac{Dt}{\pi}} - 2\sqrt{\frac{D}{\pi}}\int_0^{\sqrt{t}} c_s \, \mathrm{d}(\sqrt{t-\tau}) \quad (1)$$

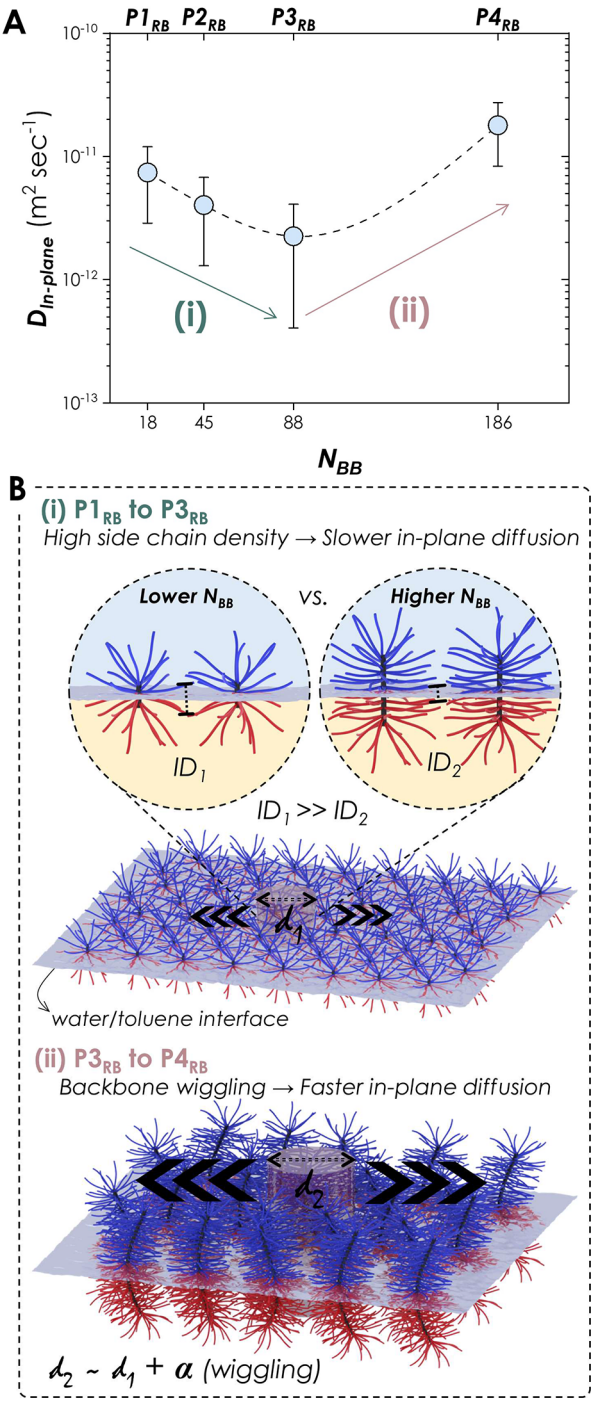

Figure 5. (A) *In-plane* diffusion coefficients obtained from FRAP experiments with different N_{BB} ($\mathbf{P1_{RB}}$-$\mathbf{P4_{RB}}$) after aging the emulsions for 1 day. (B) Schematic illustrations of two different scenarios as a function of N_{BB} of BBCPs, where (i) the increasing side-chain density near the block junctions hinders *in-plane* diffusion due to increased steric repulsion between bottlebrush polymers, and (ii) backbone wiggling (when $N_{BB} \gg N_{SC}$) provides additional space for *in-plane* diffusion.

https://doi.org/10.1021/jacs.3c13817
J. Am. Chem. Soc. 2024, 146, 13000–13009

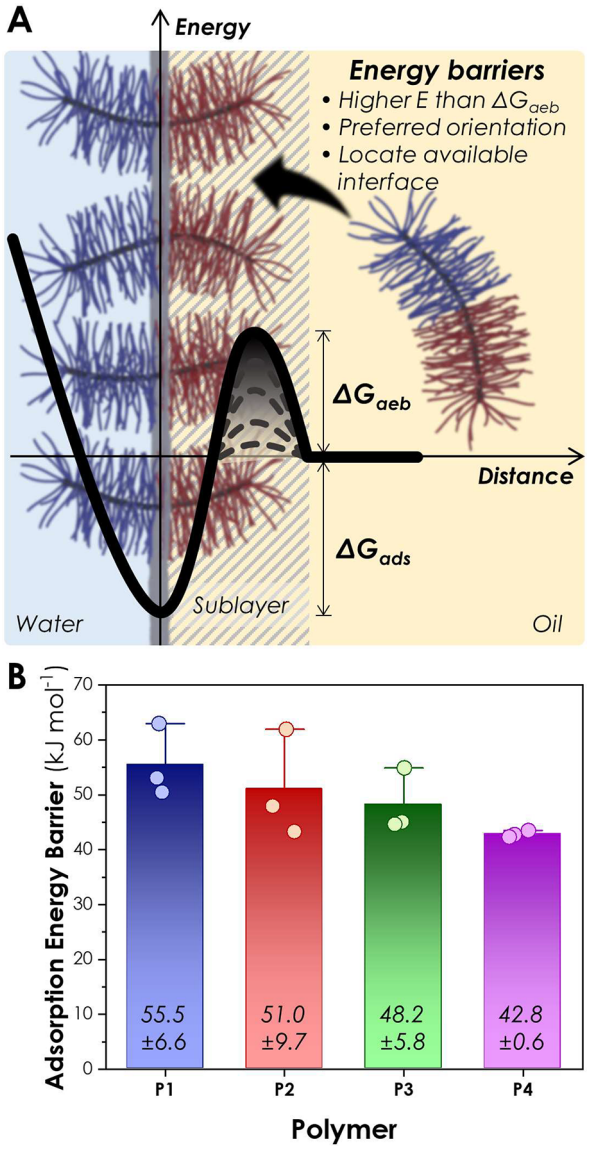

Figure 6. (A) Schematic energy diagram of BBCPs either in the bulk or at the water/toluene interface. The two free energy change, ΔG_{aeb} (adsorption energy barrier) and ΔG_{ads} (energy gain upon BBCP adsorption) represent the adsorption energy barrier and energy gain by placing the BBCP from the bulk, respectively. (B) Average ΔG_{aeb} as a function of N_{BB}.

where Γ defines BBCP surface coverage at the fluid interface, c_0 denotes BBCP concentration in the oil phase, D is the effective diffusion coefficient, c_s represents BBCP subsurface concentration, and τ is an arbitrary dummy variable of integration. Solving eq 1 requires two boundary conditions: (i) a short time approximation, $t \to 0$ and (ii) a long time approximation (equilibrium stage, $t \to \infty$). We only consider the latter, due to convection caused by injection of the water droplet during the initial interfacial tension measurement ($t \to 0$), which complicates the diffusivity calculation and the origin of assembly dynamics.[71] By using the Gibbs isotherm ($d\gamma = -nRT\Gamma\, d\ln c$, where R is the gas constant, T is the temperature in Kelvin, and $n = 1$ for nonionic surfactants),[72] taking the limit $\Delta c \to 0$ ($\Delta c = c_0 - c_s$, where c_0 is BBCP bulk concentration and c_s is concentration of BBCP in the sublayer), it can be written as

$$\gamma_t = \gamma_{eq} + \frac{RT\Gamma_{eq}^2}{c}\sqrt{\frac{\pi}{4Dt}} \tag{2}$$

To calculate the effective diffusion coefficient (D_{eff}), we first obtain Γ_{eq} from the Gibbs isotherm using the equation $\Gamma_{eq} = -(RT)^{-1}d\gamma(d\ln c)^{-1}$ at various molar concentrations (Figure 16A–D). Next, we plotted γ vs $(\text{time})^{-1/2}$ from Figure S15 and determining the slope of the plot at $t \to \infty$ (Figure S16E–H), we can calculate the D_{eff} as

$$D_{eff} = \frac{\pi R^2 T^2 \Gamma_{eq}^4}{4c^2\left(\frac{d\gamma}{d(t^{-1/2})_{t\to\infty}}\right)^2} \tag{3}$$

In the context of the "*activated-diffusion mechanism*" of the adsorption barrier in the surfactant assembly, Liggieri et al.[73] used the Arrhenius-type equation ($D_{eff} = De^{-\Delta G/RT}$, D from DLS, Figure S9) to calculate ΔG_{aeb}. Figure 6B shows ΔG_{aeb} values for BBCPs **P1**–**P4**, wherein the values monotonically decrease from 55.5 ± 6.6 kJ mol^{-1} (**P1**) to 42.8 ± 0.6 kJ mol^{-1} (**P4**). To understand this trend in ΔG_{aeb}, we consider the BBCP configuration. As N_{BB} increased, the sublayer thickness also increased due to the architecture of the BBCPs (Figure 6A). However, we need to separate the effect of sublayer thickness from the trend in ΔG_{aeb} because if the sublayer thickness were the main contributing factor, **P4** with the highest N_{BB} would have the highest ΔG_{aeb}, which is counter to our observation (Figure 6B). We emphasize that the decrease in adsorption energy at higher N_{BB} values must be a consequence of backbone tilting and wiggling associated with the higher aspect ratio bottlebrush polymers, since interchain interactions alone would create a significantly larger barrier at higher N_{BB}.

As discussed above, at higher BBCP aspect ratios, tilting and wiggling at the liquid interface expose the bare water/toluene interface, resulting in an increase in γ (Figure 3C). This in turn reduces the effective density of the components and the magnitude of nonfavorable interactions experienced by approaching BBCPs, consequently lowering ΔG_{aeb}. When the PEO block penetrates into the PDMS block of the BBCPs at the liquid interface, the incoming BBCP experiences a repulsive force. When the PEO block reaches the liquid interface, it is drawn into the water phase until the junction point localized at the water/toluene interface to minimize free energy (Figure 6A). For further context, a comparative analysis of BBCP interfacial adsorption to that of ligand-functionalized nanoparticles and conventional diblock copolymers is presented in Figure S17. We note that upon full insertion of the BBCP into the interfacial assembly the interfacial tension and the free energy are decreased, so ΔG_{ads} is negative.

CONCLUSION

In summary, we describe the N_{BB}-dependent fluid–fluid interfacial assembly kinetics, packing efficiency, *in-plane* dynamics, and adsorption energy barrier of bottlebrush block copolymer surfactants. The change of macromolecular configuration in solution proved critical in describing the interfacial assembly behavior. Equilibrium γ increased with N_{BB}, which indicates lower interfacial coverage at higher N_{BB}. For **P1**, spontaneous emulsification was induced by interfacial instabilities, reflecting a lower bending rigidity at a lower N_{BB}. The decreasing ASC with N_{BB} suggests that the BBCPs with

https://doi.org/10.1021/jacs.3c13817
J. Am. Chem. Soc. 2024, 146, 13000–13009

higher N_{BB} adopt a tilted configuration, or undergo backbone wiggling, exposing bare water/toluene interface and reducing ASC. Reducing [BBCP] to 0.001 mg mL^{-1} allowed direct comparison to equilibrium γ, τ_A, and τ_R of the BBCPs with the BRCPs containing similar side-chain chemistry. BRCPs showed increasing equilibrium γ with N_{BB}, while the BBCP γ values plateaued, demonstrating that the backbone orientations of the BRCPs and BBCPs are parallel and perpendicular to the water/toluene interface, respectively. τ_A and τ_R, determined by fitting a sum of two exponential relaxation functions to the dynamic γ plots, initially increased with N_{BB} (**P1** to **P3**), attributed to the larger R_h, slower solution diffusion, and smaller cross-sectional diameter of side-chains near the bottlebrush block junction, which impedes reorganization. However, both τ_A and τ_R decreased as N_{BB} increased further to 190 (**P4**), which is attributed to increased segregation strength and exposure of a new water/toluene interface due to the backbone wiggling and enhanced reorganization. These results were further confirmed by FRAP experiments, where the *in-plane* diffusion coefficients decreased as N_{BB} grew from 19 to 92, but increased at N_{BB} 190, sharing the same trend as τ_R. The adsorption energy barriers for BBCPs with different N_{BB} values were calculated, showing a correlation between the ΔG_{aeb} and chain configuration, i.e., backbone tilting and wiggling at the fluid interface. Overall, the assembly behavior of BBCPs at different N_{BB}:N_{SC} ratios provides invaluable insight into the design of tailored macromolecular systems in fluids. By understanding the interplay between the N_{BB}:N_{SC} ratios and the bottlebrush chain configurations, we enable informed decisions on selecting the optimal macromolecular architecture for particular applications. A deeper understanding of how BBCP shape and configuration affects macroscopic physical properties at fluid interfaces is vital for future applications of these types of macromolecular surfactants. Overall, this study establishes general design rules that guide consideration of BBCPs as surfactants, empowering researchers to harness their unique properties and tailor the performance of systems with precision.

■ ASSOCIATED CONTENT

Supporting Information

The Supporting Information is available free of charge at https://pubs.acs.org/doi/10.1021/jacs.3c13817.

Synthesis, experimental procedures, characterization data, NMR spectra, kinetic study data, f_{PEO} (PEO mole %) calculation, SEC and MALLS-SEC traces, macromonomer M_n values, structure diagram, UV−vis spectra data, size distributions, dynamic light scattering data and analysis, Zimm plots, intrinsic viscosity vs polymer concentration, rate of change of γ extracted from the γ vs time plots, fitting results for γ vs time plots, chemical structure of the fluorescence-labeled BBCPs and snapshots of the fluorescence recovery after photobleaching, equilibrium γ vs BBCP concentration, dynamic γ vs $t^{-1/2}$ at different BBCP concentrations, average ΔG_{aeb} of BBCPs (PDF)

■ AUTHOR INFORMATION

Corresponding Authors

Todd Emrick − *Polymer Science & Engineering Department, Conte Center for Polymer Research, University of Massachusetts, Amherst, Massachusetts 01003, United States;* orcid.org/0000-0003-0460-1797; Email: tsemrick@mail.pse.umass.edu

Thomas P. Russell − *Polymer Science & Engineering Department, Conte Center for Polymer Research, University of Massachusetts, Amherst, Massachusetts 01003, United States; Materials Sciences Division, Lawrence Berkeley National Laboratory, Berkeley, California 94720, United States;* orcid.org/0000-0001-6384-5826; Email: russell@mail.pse.umass.edu

Authors

Hong-Gyu Seong − *Polymer Science & Engineering Department, Conte Center for Polymer Research, University of Massachusetts, Amherst, Massachusetts 01003, United States*

Zichen Jin − *Polymer Science & Engineering Department, Conte Center for Polymer Research, University of Massachusetts, Amherst, Massachusetts 01003, United States*

Zhan Chen − *Polymer Science & Engineering Department, Conte Center for Polymer Research, University of Massachusetts, Amherst, Massachusetts 01003, United States*

Mingqiu Hu − *Polymer Science & Engineering Department, Conte Center for Polymer Research, University of Massachusetts, Amherst, Massachusetts 01003, United States;* orcid.org/0000-0003-1397-0180

Complete contact information is available at: https://pubs.acs.org/10.1021/jacs.3c13817

Notes

The authors declare no competing financial interest.

■ ACKNOWLEDGMENTS

This work was supported by the Army Research Office (W911NF-24-2-0041) with additional support for polymer synthesis from NSF-CBET-2136955.

■ REFERENCES

(1) Stadler, B.; Chandrawati, R.; Price, A. D.; Chong, S. F.; Breheney, K.; Postma, A.; Connal, L. A.; Zelikin, A. N.; Caruso, F. A microreactor with thousands of subcompartments: enzyme-loaded liposomes within polymer capsules. *Angew. Chem., Int. Ed.* **2009**, *48* (24), 4359−4362.

(2) Wang, Y.; Zhao, Q.; Haag, R.; Wu, C. Biocatalytic Synthesis Using Self-Assembled Polymeric Nano- and Microreactors. *Angew. Chem., Int. Ed.* **2022**, *61* (52), e202213974.

(3) Müllner, M.; Müller, A. H. E. Cylindrical polymer brushes - Anisotropic building blocks, unimolecular templates and particulate nanocarriers. *Polymer* **2016**, *98*, 389−401.

(4) Huang, K.; Rzayev, J. Well-Defined Organic Nanotubes from Multicomponent Bottlebrush Copolymers. *J. Am. Chem. Soc.* **2009**, *131* (19), 6880−6885.

(5) Huang, K.; Rzayev, J. Charge and size selective molecular transport by amphiphilic organic nanotubes. *J. Am. Chem. Soc.* **2011**, *133* (42), 16726−16729.

(6) Fenyves, R.; Schmutz, M.; Horner, I. J.; Bright, F. V.; Rzayev, J. Aqueous self-assembly of giant bottlebrush block copolymer surfactants as shape-tunable building blocks. *J. Am. Chem. Soc.* **2014**, *136* (21), 7762−7770.

(7) Pang, X.; He, Y.; Jung, J.; Lin, Z. 1D nanocrystals with precisely controlled dimensions, compositions, and architectures. *Science* **2016**, *353* (6305), 1268−1272.

(8) Chen, X.; Yang, X.; Song, D.-P.; Men, Y.-F.; Li, Y. Discovery and Insights into Organized Spontaneous Emulsification via Interfacial Self-Assembly of Amphiphilic Bottlebrush Block Copolymers. *Macromolecules* **2021**, *54* (8), 3668−3677.

(9) Torchilin, V. Structure and design of polymeric surfactant-based drug delivery systems. *J. Controlled Release* **2001**, *73* (2−3), 137−172.
(10) Johnson, J. A.; Lu, Y. Y.; Burts, A. O.; Lim, Y.-H.; Finn, M. G.; Koberstein, J. T.; Turro, N. J.; Tirrell, D. A.; Grubbs, R. H. Core-Clickable PEG-Branch-Azide Bivalent-Bottle-Brush Polymers by ROMP: Grafting-Through and Clicking-To. *J. Am. Chem. Soc.* **2011**, *133* (3), 559−566.
(11) Johnson, J. A.; Lu, Y. Y.; Burts, A. O.; Xia, Y.; Durrell, A. C.; Tirrell, D. A.; Grubbs, R. H. Drug-loaded, bivalent-bottle-brush polymers by graft-through ROMP. *Macromolecules* **2010**, *43* (24), 10326−10335.
(12) Dalal, R. J.; Kumar, R.; Ohnsorg, M.; Brown, M.; Reineke, T. M. Cationic Bottlebrush Polymers Outperform Linear Polycation Analogues for pDNA Delivery and Gene Expression. *ACS Macro Lett.* **2021**, *10* (7), 886−893.
(13) Corredor, L. M.; Husein, M. M.; Maini, B. B. A review of polymer nanohybrids for oil recovery. *Adv. Colloid Interface Sci.* **2019**, *272*, 102018.
(14) Raffa, P.; Broekhuis, A. A.; Picchioni, F. Polymeric surfactants for enhanced oil recovery: A review. *J. Pet. Sci. Eng.* **2016**, *145*, 723−733.
(15) ShamsiJazeyi, H.; Miller, C. A.; Wong, M. S.; Tour, J. M.; Verduzco, R. Polymer coated nanoparticles for enhanced oil recovery. *J. Appl. Polym. Sci.* **2014**, *131* (15), 40576.
(16) Caruso, F.; Trau, D.; Mohwald, H.; Renneberg, R. Enzyme Encapsulation in Layer-by-Layer Engineered Polymer Multilayer Capsules. *Langmuir* **2000**, *16* (4), 1485−1488.
(17) Li, K.; Liu, B. Polymer-encapsulated organic nanoparticles for fluorescence and photoacoustic imaging. *Chem. Soc. Rev.* **2014**, *43* (18), 6570−6597.
(18) Villemin, E.; Ong, Y. C.; Thomas, C. M.; Gasser, G. Polymer encapsulation of ruthenium complexes for biological and medicinal applications. *Nat. Rev. Chem.* **2019**, *3* (4), 261−282.
(19) Hu, M.; Russell, T. P. Polymers with advanced architectures as emulsifiers for multi-functional emulsions. *Mater. Chem. Front.* **2021**, *5* (3), 1205−1220.
(20) Alexandridis, P.; Hatton, T. A. Poly(ethylene oxide)-poly-(propylene oxide)-poly (ethylene oxide) block copolymer surfactants in aqueous solutions and at interfaces: thermodynamics, structure, dynamics, and modeling. *Colloids Surf., A* **1995**, *96*, 1−46.
(21) Alexandridis, P. Poly(ethylene oxide)/poly(propylene oxide) block copolymer Surfactants. *Curr. Opin. Colloid Interface Sci.* **1997**, *2* (5), 478−489.
(22) Yeung, C.; Balazs, A. C.; Jasnow, D. Adsorption of Copolymer Chains at Liquid-Liquid Interfaces: Effect of Sequence Distribution. *Macromolecules* **1992**, *25* (4), 1357−1360.
(23) Leclerc, E.; Daoud, M. Multiblock Copolymers at Interfaces: Concentration and Selectivity Effects. *Macromolecules* **1997**, *30* (2), 293−300.
(24) Jimenez-Angeles, F.; Kwon, H. K.; Sadman, K.; Wu, T.; Shull, K. R.; Olvera de la Cruz, M. Self-Assembly of Charge-Containing Copolymers at the Liquid-Liquid Interface. *ACS Cent. Sci.* **2019**, *5* (4), 688−699.
(25) Yuan, Q.; Russell, T. P.; Wang, D. Self-Assembly Behavior of PS-b-P2VP Block Copolymers and Carbon Quantum Dots at Water/Oil Interfaces. *Macromolecules* **2020**, *53* (24), 10981−10987.
(26) Chen, Z.; Hu, M.; Li, X.; Smith, D. M.; Seong, H. G.; Emrick, T.; Rzayev, J.; Russell, T. P. In Situ Hydrolysis of Block Copolymers at the Water-Oil Interface. *Angew. Chem., Int. Ed.* **2022**, *61* (25), e202201392.
(27) Carrillo, J. Y.; Chen, Z.; Premadasa, U. I.; Steinmetz, C.; Coughlin, E. B.; Doughty, B.; Russell, T. P.; Sumpter, B. G. Assembly of polyelectrolyte star block copolymers at the oil-water interface. *Nanoscale* **2023**, *15* (3), 1042−1052.
(28) Seong, H.-G.; Chen, Z.; Emrick, T.; Russell, T. P. Reconfiguration and Reorganization of Bottlebrush Polymer Surfactants. *Angew. Chem., Int. Ed.* **2022**, *61* (19), e202200530.
(29) Seong, H.-G.; Fink, Z.; Chen, Z.; Emrick, T.; Russell, T. P. Bottlebrush Polymers at Liquid Interfaces: Assembly Dynamics, Mechanical Properties, and All-Liquid Printed Constructs. *ACS Nano* **2023**, *17* (15), 14731−14741.
(30) Xie, G.; Krys, P.; Tilton, R. D.; Matyjaszewski, K. Heterografted Molecular Brushes as Stabilizers for Water-in-Oil Emulsions. *Macromolecules* **2017**, *50* (7), 2942−2950.
(31) Li, Y.; Zou, J.; Das, B. P.; Tsianou, M.; Cheng, C. Well-Defined Amphiphilic Double-Brush Copolymers and Their Performance as Emulsion Surfactants. *Macromolecules* **2012**, *45* (11), 4623−4629.
(32) Wang, B.; Liu, T.; Chen, H.; Yin, B.; Zhang, Z.; Russell, T. P.; Shi, S. Molecular Brush Surfactants: Versatile Emulsifiers for Stabilizing and Structuring Liquids. *Angew. Chem., Int. Ed.* **2021**, *60* (36), 19626−19630.
(33) Hsieh, T. L.; Martinez, M. R.; Garoff, S.; Matyjaszewski, K.; Tilton, R. D. Interfacial dilatational rheology as a bridge to connect amphiphilic heterografted bottlebrush copolymer architecture to emulsifying efficiency. *J. Colloid Interface Sci.* **2021**, *581*, 135−147.
(34) Sheiko, S. S.; Sumerlin, B. S.; Matyjaszewski, K. Cylindrical molecular brushes: Synthesis, characterization, and properties. *Prog. Polym. Sci.* **2008**, *33* (7), 759−785.
(35) Rzayev, J. Molecular Bottlebrushes: New Opportunities in Nanomaterials Fabrication. *ACS Macro Lett.* **2012**, *1* (9), 1146−1149.
(36) Verduzco, R.; Li, X.; Pesek, S. L.; Stein, G. E. Structure, function, self-assembly, and applications of bottlebrush copolymers. *Chem. Soc. Rev.* **2015**, *44* (8), 2405−2420.
(37) Li, Z.; Tang, M.; Liang, S.; Zhang, M.; Biesold, G. M.; He, Y.; Hao, S.-M.; Choi, W.; Liu, Y.; Peng, J.; Lin, Z. Bottlebrush polymers: From controlled synthesis, self-assembly, properties to applications. *Prog. Polym. Sci.* **2021**, *116*, 101387.
(38) Zhulina, E. B.; Sheiko, S. S.; Borisov, O. V. Theoretical advances in molecular bottlebrushes and comblike (co)polymers: solutions, gels, and self-assembly. *Soft Matter* **2022**, *18* (46), 8714−8732.
(39) Rzayev, J. Synthesis of Polystyrene-Polylactide Bottlebrush Block Copolymers and Their Melt Self-Assembly into Large Domain Nanostructures. *Macromolecules* **2009**, *42* (6), 2135−2141.
(40) Gu, W.; Huh, J.; Hong, S. W.; Sveinbjornsson, B. R.; Park, C.; Grubbs, R. H.; Russell, T. P. Self-Assembly of Symmetric Brush Diblock Copolymers. *ACS Nano* **2013**, *7* (3), 2551−2558.
(41) Dalsin, S. J.; Rions-Maehren, T. G.; Beam, M. D.; Bates, F. S.; Hillmyer, M. A.; Matsen, M. W. Bottlebrush Block Polymers: Quantitative Theory and Experiments. *ACS Nano* **2015**, *9* (12), 12233−12245.
(42) Hu, M.; Li, X.; Rzayev, J.; Russell, T. P. Hydrolysis-Induced Self-Assembly of High-χ-Low-N Bottlebrush Copolymers. *Macromolecules* **2021**, *54* (24), 11449−11458.
(43) Hong, S. W.; Gu, W.; Huh, J.; Sveinbjornsson, B. R.; Jeong, G.; Grubbs, R. H.; Russell, T. P. On the Self-Assembly of Brush Block Copolymers in Thin Films. *ACS Nano* **2013**, *7* (11), 9684−9692.
(44) Pesek, S. L.; Li, X.; Hammouda, B.; Hong, K.; Verduzco, R. Small-Angle Neutron Scattering Analysis of Bottlebrush Polymers Prepared via Grafting-Through Polymerization. *Macromolecules* **2013**, *46* (17), 6998−7005.
(45) Dutta, S.; Wade, M. A.; Walsh, D. J.; Guironnet, D.; Rogers, S. A.; Sing, C. E. Dilute solution structure of bottlebrush polymers. *Soft Matter* **2019**, *15* (14), 2928−2941.
(46) Fenyves, R.; Schmutz, M.; Horner, I. J.; Bright, F. V.; Rzayev, J. Aqueous self-assembly of giant bottlebrush block copolymer surfactants as shape-tunable building blocks. *J. Am. Chem. Soc.* **2014**, *136* (21), 7762−7770.
(47) Patel, B. B.; Pan, T.; Chang, Y.; Walsh, D. J.; Kwok, J. J.; Park, K. S.; Patel, K.; Guironnet, D.; Sing, C. E.; Diao, Y. Concentration-Driven Self-Assembly of PS-b-PLA Bottlebrush Diblock Copolymers in Solution. *ACS Polym. Au* **2022**, *2* (4), 232−244.
(48) Ma, H.; Kim, K. T. Self-Assembly of Bottlebrush Block Copolymers into Triply Periodic Nanostructures in a Dilute Solution. *Macromolecules* **2020**, *53* (2), 711−718.
(49) Lebedeva, I. O.; Zhulina, E. B.; Borisov, O. V. Self-Assembly of Bottlebrush Block Copolymers in Selective Solvent: Micellar Structures. *Polymers* **2021**, *13* (9), 1351.

https://doi.org/10.1021/jacs.3c13817
J. Am. Chem. Soc. 2024, 146, 13000−13009

(50) Kim, E. J.; Shin, J. J.; Do, T.; Lee, G. S.; Park, J.; Thapar, V.; Choi, J.; Bang, J.; Yi, G. R.; Hur, S. M.; Kim, J. G.; Kim, B. J. Molecular Weight Dependent Morphological Transitions of Bottlebrush Block Copolymer Particles: Experiments and Simulations. *ACS Nano* **2021**, *15* (3), 5513−5522.
(51) Li, Y. L.; Chen, X.; Geng, H. K.; Dong, Y.; Wang, B.; Ma, Z.; Pan, L.; Ma, G. Q.; Song, D. P.; Li, Y. S. Oxidation Control of Bottlebrush Molecular Conformation for Producing Libraries of Photonic Structures. *Angew. Chem., Int. Ed.* **2021**, *60* (7), 3647−3653.
(52) Alaboalirat, M.; Qi, L.; Arrington, K. J.; Qian, S.; Keum, J. K.; Mei, H.; Littrell, K. C.; Sumpter, B. G.; Carrillo, J.-M. Y.; Verduzco, R.; Matson, J. B. Amphiphilic Bottlebrush Block Copolymers: Analysis of Aqueous Self-Assembly by Small-Angle Neutron Scattering and Surface Tension Measurements. *Macromolecules* **2019**, *52* (2), 465−476.
(53) Nam, J.; Kim, Y.; Kim, J. G.; Seo, M. Self-Assembly of Monolayer Vesicles via Backbone-Shiftable Synthesis of Janus Core-Shell Bottlebrush Polymer. *Macromolecules* **2019**, *52* (24), 9484−9494.
(54) He, Q.; Ku, K. H.; Vijayamohanan, H.; Kim, B. J.; Swager, T. M. Switchable Full-Color Reflective Photonic Ellipsoidal Particles. *J. Am. Chem. Soc.* **2020**, *142* (23), 10424−10430.
(55) Foster, J. C.; Varlas, S.; Couturaud, B.; Coe, Z.; O'Reilly, R. K. Getting into Shape: Reflections on a New Generation of Cylindrical Nanostructures' Self-Assembly Using Polymer Building Blocks. *J. Am. Chem. Soc.* **2019**, *141* (7), 2742−2753.
(56) Fielden, S. D. P.; Derry, M. J.; Miller, A. J.; Topham, P. D.; O'Reilly, R. K. Triggered Polymersome Fusion. *J. Am. Chem. Soc.* **2023**, *145* (10), 5824−5833.
(57) Ahmed, E.; Womble, C. T.; Weck, M. Synthesis and Aqueous Self-Assembly of ABCD Bottlebrush Block Copolymers. *Macromolecules* **2020**, *53* (20), 9018−9025.
(58) Pan, T.; Dutta, S.; Kamble, Y.; Patel, B. B.; Wade, M. A.; Rogers, S. A.; Diao, Y.; Guironnet, D.; Sing, C. E. Materials Design of Highly Branched Bottlebrush Polymers at the Intersection of Modeling, Synthesis, Processing, and Characterization. *Chem. Mater.* **2022**, *34* (5), 1990−2024.
(59) Love, J. A.; Morgan, J. P.; Trnka, T. M.; Grubbs, R. H. A practical and highly active ruthenium-based catalyst that effects the cross metathesis of acrylonitrile. *Angew. Chem., Int. Ed.* **2002**, *41* (21), 4035−4037.
(60) Vougioukalakis, G. C.; Grubbs, R. H. Ruthenium-Based Heterocyclic Carbene-Coordinated Olefin Metathesis Catalysts. *Chem. Rev.* **2010**, *110*, 1746−1787.
(61) Siirilä, J.; Häkkinen, S.; Tenhu, H. The emulsion polymerization induced self-assembly of a thermoresponsive polymer poly(N-vinylcaprolactam). *Polym. Chem.* **2019**, *10* (6), 766−775.
(62) Colby, R. H.; Rubinstein, M. *Polymer Physics*; Oxford University, 2003.
(63) Huber, K.; Burchard, W.; Fetters, L. J. Dynamic Light Scattering from Regular Star-Branched Molecules. *Macromolecules* **1984**, *17* (4), 541−548.
(64) Berry, J. D.; Neeson, M. J.; Dagastine, R. R.; Chan, D. Y.; Tabor, R. F. Measurement of surface and interfacial tension using pendant drop tensiometry. *J. Colloid Interface Sci.* **2015**, *454*, 226−237.
(65) Hasnain, J.; Jiang, Y.; Hou, H.; Yan, J.; Athanasopoulou, L.; Forth, J.; Ashby, P. D.; Helms, B. A.; Russell, T. P.; Geissler, P. L. Spontaneous emulsification induced by nanoparticle surfactants. *J. Chem. Phys.* **2020**, *153* (22), 224705.
(66) Ku, K. H.; Shin, J. M.; Klinger, D.; Jang, S. G.; Hayward, R. C.; Hawker, C. J.; Kim, B. J. Particles with Tunable Porosity and Morphology by Controlling Interfacial Instability in Block Copolymer Emulsions. *ACS Nano* **2016**, *10* (5), 5243−5251.
(67) Panyukov, S.; Zhulina, E. B.; Sheiko, S. S.; Randall, G. C.; Brock, J.; Rubinstein, M. Tension Amplification in Molecular Brushes in Solutions and on Substrates. *J. Phys. Chem. B* **2009**, *113* (12), 3750−3768.
(68) Loren, N.; Hagman, J.; Jonasson, J. K.; Deschout, H.; Bernin, D.; Cella-Zanacchi, F.; Diaspro, A.; McNally, J. G.; Ameloot, M.; Smisdom, N.; Nyden, M.; Hermansson, A. M.; Rudemo, M.; Braeckmans, K. Fluorescence recovery after photobleaching in material and life sciences: putting theory into practice. *Q. Rev. Biophys.* **2015**, *48* (3), 323−87.
(69) Luo, Y.; Kim, B.; Montarnal, D.; Mester, Z.; Pester, C. W.; McGrath, A. J.; Hill, G.; Kramer, E. J.; Fredrickson, G. H.; Hawker, C. J. Improved self assembly of poly(dimethylsiloxane b ethylene oxide) using a hydrogen bonding additive. *J. Polym. Sci., Part A: Polym. Chem.* **2016**, *54* (14), 2200−2208.
(70) Ward, A. F. H.; Tordai, L. Time-Dependence of Boundary Tensions of Solutions I. The Role of Diffusion in Time-Effects. *J. Chem. Phys.* **1946**, *14* (7), 453−461.
(71) Chen, D.; Sun, Z.; Russell, T. P.; Jin, L. Coassembly Kinetics of Graphene Oxide and Block Copolymers at the Water/Oil Interface. *Langmuir* **2017**, *33* (36), 8961−8969.
(72) Eastoe, J.; Dalton, J. S. Dynamic surface tension and adsorption mechanisms of surfactants at the air-water interface. *Adv. Colloid Interface Sci.* **2000**, *85* (2−3), 103−144.
(73) Ravera, F.; Liggieri, L.; Steinchen, A. Sorption Kinetics Considered as a Renormalized Diffusion Process. *J. Colloid Interface Sci.* **1993**, *156*, 109−116.

https://doi.org/10.1021/jacs.3c13817
J. Am. Chem. Soc. 2024, 146, 13000−13009